

Cite this: *Polym. Chem.*, 2026, **17**, 1837

# Degrating reaction of polymer brushes: the determining role of molecular weight and grafting density

Riccardo Chiarcos,<sup>a</sup>  \*<sup>a</sup> Diego Antonioli,<sup>a</sup> Luca Gabutti,<sup>a</sup> Elo Marsengo,<sup>a</sup> Michele Perego <sup>b</sup> and Michele Laus<sup>a</sup>

The chemical stability of polymer brushes is mandatory to ensure their applicability in a wide range of environments. However, it is well-known that, in the presence of water, polymer chains detach from the substrate due to the hydrolytic cleavage of the anchoring bonds at the polymer–substrate interface. Furthermore, this degrafting reaction is promoted by the tension generated on the labile anchoring bonds by the swelling of the brush. It is now widely demonstrated that the brush tension increases, speeding up the degrafting reaction, as the number of chains per unit area (grafting density) increases. In contrast, the role of the molecular weight of the grafted polymer in the degrafting reaction is much less investigated. In this work, polymer brushes made up of polystyrenes with different molecular weights were obtained by the grafting to approach. Chain degrafting was then induced by a THF/water mixture and the progress of the degrafting reaction was followed by thickness measurements on the dry brushes. The reaction rate constant of the degrafting process was calculated as a function of both the grafting density and the molecular weight of the polymer, confirming that both parameters have a significant role. Furthermore, the degrafting reaction was also evaluated in brushes containing long and short chains in different percentages. A reciprocal influence was observed between the two components, with the overall degrafting process being precisely dictated by the predominant one.

Received 23rd December 2025,  
Accepted 6th April 2026

DOI: 10.1039/d5py01210d

rsc.li/polymers

## Introduction

Adaptable and programmable surfaces are highly required in all those applications in which the interaction between a material and the surrounding environment is critical.<sup>1</sup> Among the tools of surface engineering, polymer brush technology is certainly the most promising.<sup>2–4</sup> In fact, polymer brushes, which consist of polymer chains chemically anchored by one end to a substrate, are currently evaluated for a broad range of applications such as sensing,<sup>5–7</sup> electronics,<sup>8–12</sup> membranes,<sup>13,14</sup> adhesives,<sup>15,16</sup> energy devices,<sup>17</sup> lubricants,<sup>18–21</sup> biocompatible coatings,<sup>22,23</sup> and bioscience.<sup>3,24–26</sup>

Polymer brushes are generally obtained through two distinct approaches: grafting from and grafting to.<sup>4,27</sup> In grafting from, the substrate is initially reacted with a functional initiator and then the polymer chains are grown from the substrate dipped in a monomer solution.<sup>28</sup> Although several polymerization techniques are suitable for the grafting from

approach, the most common is undoubtedly the Surface Initiated-Atom Transfer Radical Polymerization (SI-ATRP), which allows several monomers to be polymerized and leads to polymers with controlled molecular weights and relatively narrow weight distributions.<sup>29–34</sup> The grafting from approach is certainly the most suited for the synthesis of brushes with high grafting densities ( $\Sigma$ , number of chains per unit area) and thicknesses ( $H$ ). However, the need to detach the grafted chains, also taking into account their very low amounts, makes their characterization non-trivial. Conversely, in the grafting to process, polymers with functional end-groups are synthesized, fully characterized and then chemically attached to the substrate.<sup>35</sup> The drawback of this approach is the limited grafting density that can be achieved due to the self-limiting nature of the grafting to reaction.<sup>36</sup> In fact, it has been widely demonstrated that the maximum obtainable values of both  $H$  and  $\Sigma$  of a brush obtained by grafting to depend on the molecular weight of the grafted polymer.<sup>37–41</sup> Interestingly, this relationship between the maximum grafting density achievable and the molecular weight of the polymer was recently exploited for silicon doping applications in microelectronics.<sup>12,42,43</sup>

If grafting reactions are the tools that enable brush synthesis, the reverse process, generally called degrafting, deserves no less attention.<sup>27</sup> For example, the self-limiting

<sup>a</sup>Department of Science and Technological Innovation (DISIT), Università del Piemonte Orientale (UPO), Alessandria 15121, Italy.

E-mail: riccardo.chiarcos@uniupo.it

<sup>b</sup>Institute for Microelectronics and Microsystems (IMM), National Research Council of Italy (CNR), Agrate Brianza 20864, Italy





ing polymers with different molecular weights is still lacking, despite their common use in applications.

In the present work, the degrafting of polystyrene brushes obtained by grafting to was investigated in a tetrahydrofuran (THF) solution containing water. The use of polystyrene as a model polymer is motivated by the fact that it contains neither cleavable nor ionisable groups in the main chain, which would add further variables to the study of the degrafting process. The clarification of the influence of both the molecular weight and the grafting density on the degrafting rate constant was the main focus of this work and was thus evaluated during the entire degrafting process. Furthermore, bimodal brushes containing different amounts of short and long polymers were also investigated with the aim to evaluate degrafting in disperse systems. The degrafting rate constants of the short and long components of the brush were determined and evaluated as a function of the brush composition.

## Results and discussion

A hydroxy-terminated deuterated polystyrene with a number average molecular weight ( $M_n$ ) of 5.2 kg mol<sup>-1</sup> (dispersity index  $D = 1.12$ ) and two hydroxy-terminated hydrogenated polystyrenes with  $M_n$  of 13 kg mol<sup>-1</sup> ( $D = 1.06$ ) and 43.2 kg mol<sup>-1</sup> ( $D = 1.16$ ) were synthesized by the ARGET-ATRP (Activator ReGenerated by Electron Transfer-Atom Transfer Radical Polymerization) technique.<sup>41,42,66</sup> More details on the synthesis and characterization are published elsewhere.<sup>45</sup> The three samples are indicated as PS<sub>d8</sub>5.2-OH, PS13-OH and PS43.2-OH, respectively.

### Degrfting reaction in single polymer brushes

Polymer brushes consisting of either PS<sub>d8</sub>5.2-OH, PS13-OH or PS43.2-OH were obtained by the grafting to approach on silicon wafer substrates covered by an ~2 nm thick layer of native oxide (SiO<sub>2</sub>). The scheme of the reaction is represented in Fig. 1 and consists of a condensation reaction between the hydroxyl end-group of the polystyrene and the surface silanols.<sup>46</sup> In detail, a thin layer (30 nm) of the functional polymer was deposited by spin-coating on the substrate and the grafting to reaction was performed at 250 °C for 900 s under melt conditions and under an inert atmosphere. The reaction conditions were selected to achieve the maximum values of  $H$  and  $\Sigma$ , in accordance with the self-limiting nature of the process.<sup>45,46</sup> The unreacted chains were removed by toluene washes and the thickness of the dry brush was evaluated by

ellipsometry. A representation of the overall process is included in the SI (see Fig. S1). The average thickness of the obtained brushes ( $H_0$ ) was 4.3, 7.6 and 14.5 nm when PS<sub>d8</sub>5.2-OH, PS13-OH and PS43.2-OH were used, respectively. The grafting densities of the brushes were also calculated using eqn (2),<sup>67</sup>

$$\Sigma = \frac{HdN_A}{M_n} \quad (2)$$

where  $H$  is the brush thickness,  $d$  is the polymer density,  $N_A$  is the Avogadro's number and  $M_n$  is the average molecular weight of the grafted polymer. The average grafting densities ( $\Sigma_0$ ) were 0.52, 0.37 and 0.21 chains per nm<sup>2</sup> for PS<sub>d8</sub>5.2-OH, PS13-OH and PS43.2-OH brushes, respectively. Both  $H_0$  and  $\Sigma_0$  values are in good accordance with the literature.<sup>45</sup>

The degrafting reaction was performed at room temperature by immersing the polymer brushes in a mixture of 75% THF and 25% of a pH = 10 buffer solution. This mixture turned out to be much more effective than either simple deionized water or pH = 10 buffer solution alone, as clearly seen in Fig. S2. The addition of THF makes the mixture significantly more affine to polystyrene, thus promoting the swelling of the brush and the access of the mixture at the polymer/substrate interface. Consistent with this, THF and water mixtures with similar percentages were already used for studying degrafting reactions.<sup>63</sup> In the present work, a pH = 10 buffer solution was used instead of pure water to speed up the reaction. The expected reaction is essentially the reverse of the grafting to reaction (see Fig. 1) and consists of the hydrolysis of the siloxane bond anchoring the polymer at the substrate.

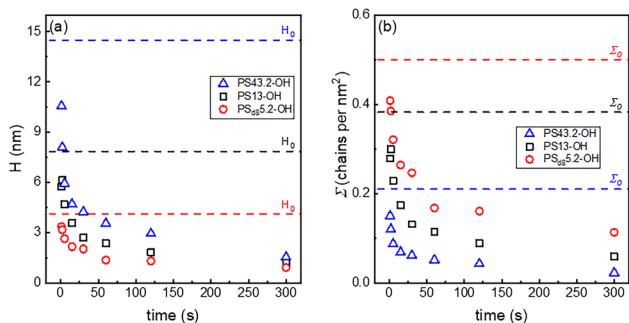
The hydrolysis of the polymer chains from the brush layer was monitored by recording the thickness of the dried brush after different times of exposure to the degrafting solution. The obtained  $H$  values are reported in Fig. 2(a). Similarly, the relative  $\Sigma$  values were calculated using eqn (2) and are reported in Fig. 2(b). Obviously,  $H$  and  $\Sigma$  present similar trends with a steep initial decrease followed by a slower decrease for long times.

It was already argued that the hydrolysis–degrafting reactions can be reasonably described by pseudo-first order kinetics, assuming that water is constant throughout the entire course of the reaction.<sup>65</sup> In this perspective approach, the reaction rate constant ( $k$ ) is estimated as the slope of the curve obtained by plotting  $\ln(\Sigma/\Sigma_0)$  as a function of the degrafting time, as reported in Fig. 3(a). The most immediate evidence is that the slope of the degrafting curve is not constant but decreases as the reaction proceeds, thus leading to a parallel

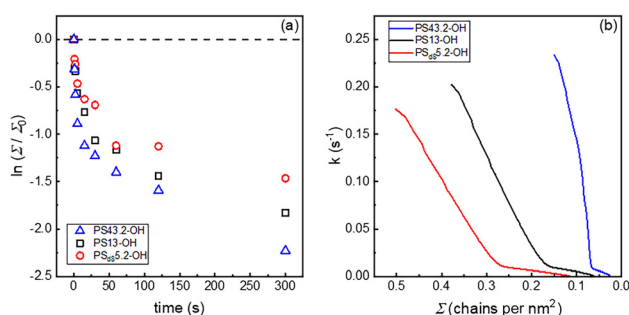


Fig. 1 Grafting to and degrafting reactions of hydroxy-terminated polystyrenes on SiO<sub>2</sub> substrates.





**Fig. 2**  $H$  (a) and  $\Sigma$  (b) values as a function of the degrafting time for the polymer brushes consisting of PS<sub>d85.2</sub>-OH (red dashes), PS13-OH (black dashes) and PS43.2-OH (blue dashes). The values of  $H_0$  and  $\Sigma_0$ , relative to the brushes before degrafting, are also included as dashed lines.



**Fig. 3**  $\ln(\Sigma/\Sigma_0)$  vs. degrafting time (a) and  $k$  vs.  $\Sigma$  (b) for the polymer brushes consisting of PS<sub>d85.2</sub>-OH (red), PS13-OH (black) and PS43.2-OH (blue).

decrease in  $k$ . This phenomenon was already described in the literature<sup>54,64</sup> and is promoted by the tension  $f$  that the swollen and stretched chains induce on the anchoring points.<sup>34</sup> Therefore, since  $f$  decreases as  $\Sigma$  decreases, as indicated in eqn (1),  $k$  is expected to decrease as the degrafting proceeds.

The value of  $k$  at each degrafting time was obtained by fitting the data reported in Fig. 3(a) and making the derivative of the obtained curve. Furthermore, to establish a direct relationship between  $k$  and  $\Sigma$  during the reaction course, at each degrafting time, the corresponding grafting density was assigned by fitting the data reported in Fig. 2(b). Finally, the values of  $k$  and  $\Sigma$  corresponding to the same degrafting time were associated, obtaining the curves reported in Fig. 3(b). More details on the fitting method are reported in the SI. The dependence of  $k$  on  $\Sigma$  is confirmed across the entire grafting density range. In more detail,  $k$  decreases as  $\Sigma$  decreases steeply at first and then, once a critical value of  $\Sigma$  ( $\Sigma_c$ ) is reached, more gradually, thus suggesting the presence of two different regimes in which the degrafting occurs.

Furthermore, for each value of  $\Sigma$ ,  $k$  is systematically higher for the polymer with a higher  $M_n$ , thus confirming that the detachment from the substrate is faster when the molecular weight is higher. This fact is particularly evident for  $\Sigma > \Sigma_c$ ,

whereas the difference being less pronounced. Finally, the value of  $\Sigma_c$  depends on the molecular weight of the polymer, with a  $\Sigma_c$  of approximately 0.27, 0.17 and 0.07 chains per nm<sup>2</sup> for PS<sub>d85.2</sub>-OH, PS13-OH and PS43.2-OH, respectively.

A reasonable interpretation of the data presented in Fig. 3(b) is that for  $\Sigma < \Sigma_c$  the grafted chains are far enough and do not significantly interact with each other. Consequently, there is a negligible tension  $f$  at the anchoring points. In contrast, for  $\Sigma > \Sigma_c$ , inter-chain interactions take place more strongly and generate the tension  $f$  which promotes the hydrolytic reaction, thus resulting in an increase in  $k$ , as predicted using eqn (1). In this study,  $\Sigma_c$  is lower for the polymer with a higher molecular weight because of its larger volume, in good accordance with the experimental evidence. A first-order estimation of the grafting density at which the polymer chains begin to overlap is given by  $1/\pi R_g^2$ , where  $R_g$  represents the radius of gyration of the polymer within the brush and  $\pi R_g^2$  is the area occupied by a single chain. As a first approximation,  $R_g$  can be calculated using eqn (3),<sup>45</sup>

$$R_g = \left(\frac{N}{6}\right)^{1/2} b \quad (3)$$

where  $N$  is the degree of polymerization and  $b$  is the statistical segment length (0.68 nm for polystyrene<sup>45</sup>). The three samples PS<sub>d85.2</sub>-OH, PS13-OH and PS43.2-OH are characterized by  $R_g$  values of 1.89, 3.10 and 5.66 nm respectively, corresponding to overlap  $\Sigma$  values of 0.09, 0.03 and 0.01 chains per nm<sup>2</sup>. Notably, eqn (3) estimates  $R_g$  of the polymer in the melt state or in a theta-solvent, whereas in the presence of a more compatible solvent,  $R_g$  may increase, leading to a subsequent decrease in the overlap  $\Sigma$  value.<sup>36</sup> In all cases, the observed  $\Sigma_c$  values are systematically higher than the expected overlap threshold. This suggests that inter-chain interactions become significant in generating tension only when the polymer brush is already partially crowded.

In any case, it should be stressed that eqn (1) is largely incomplete because it does not include a specific dependence of  $f$  on the molecular weight of the grafted polymer chain. Further research is certainly necessary to identify all the parameters involved in the degrafting process. However, what is clear is that the role of  $M_n$  cannot be ignored when polymer brushes obtained with classical grafting to approaches are subjected to degrafting.

The following section will be dedicated to the study of degrafting in disperse brushes, where long and short polymers are grafted together.

### Degrafting reaction in bimodal polymer brushes

Bimodal polymer brushes containing both PS<sub>d85.2</sub>-OH and PS13-OH were prepared by grafting to. In particular, three polymer brushes containing PS<sub>d85.2</sub>-OH at percentages of 90, 50 and 20%, indicated as Brush90, Brush50 and Brush20, were the target brushes.

It is well known that, during the grafting to reactions, polymers with lower molecular weights react preferentially with the



substrate.<sup>68–70</sup> This leads to an enrichment of short chains in the brush compared to the composition of the initial polymer mixture. In detail, when a mixture of polymer 1 and polymer 2 is grafted, the ratio between the grafting densities of the two polymers is calculated as follows:<sup>36</sup>

$$\frac{\Sigma_1}{\Sigma_2} = X \left( \frac{M_{n1}}{M_{n2}} \right)^{-0.5} \quad (4)$$

where  $\Sigma_1$  and  $\Sigma_2$  are the grafting densities of polymer 1 and polymer 2 in the brush,  $X$  is the molar ratio between polymer 1 and polymer 2 in the initial polymer mixture, and  $M_{n1}$  and  $M_{n2}$  are the average molecular weights of polymer 1 and polymer 2. According to eqn (4), if  $M_{n1} < M_{n2}$ , then  $\Sigma_1/\Sigma_2 > X$  and an enrichment of the short polymer 1 takes place in the brush. In this work, eqn (4) was applied in the reverse way to find the right value of  $X$  that is required to obtain a brush with a desired composition.

The grafting procedure was the same as described in the previous section. The thickness ( $H_0$ ) of the brushes was determined by ellipsometry, while the brush composition was investigated by TGA-GC-MS (ThermoGravimetric Analysis-Gas Chromatography-Mass Spectrometry) analysis. The TGA-GC-MS procedure is now a consolidated approach for determining the composition of polymer brushes containing different polymer species.<sup>45,71–73</sup> In this case, since the two components of the brush are polystyrenes differing in their  $M_n$  only, the contrast was produced by using a deuterated and a hydrogenated polystyrene sample. Briefly, in the TGA oven the brush was heated to promote the degradation of the polymers *via* an unzipping process that generates principally monomers.<sup>71</sup> The monomers are conveyed in an inert gas flow to a GC and analyzed in a mass detector. The intensity of the signals after proper calibration relative to deuterated styrene, for PS<sub>d8</sub>5.2-OH, and hydrogenated styrene, for PS13-OH, were combined with the measurement of  $H_0$  to determine the grafting density of PS<sub>d8</sub>5.2-OH ( $\Sigma_{D,0}$ ), the grafting density of PS13-OH ( $\Sigma_{H,0}$ ) and the total grafting density of the brush ( $\Sigma_{TOT,0} = \Sigma_{D,0} + \Sigma_{H,0}$ ).<sup>45</sup> More details on the measurements and calculations are contained in the Experimental section. The characteristics of the obtained brushes are reported in Table 1.

The degrafting procedure was the same as described in the previous section for single polymer brushes. The values of  $H$  measured after different degrafting times are reported in Fig. S6. The composition of the brushes was also determined with TGA-GC-MS analysis and  $\Sigma_D$ ,  $\Sigma_H$  and  $\Sigma_{TOT}$  are reported in Fig. 4. Both the partial and the total grafting densities follow the same trend that was already reported for the single

polymer brushes, with a rapid decrease at short degrafting times, followed by a slower decrease at longer times. The same behavior was observed for Brush90, Brush50 and Brush20.

To further explore the degrafting kinetics,  $\ln(\Sigma_D/\Sigma_{D,0})$  and  $\ln(\Sigma_H/\Sigma_{H,0})$  were reported as a function of the degrafting time for each typology of brush (see Fig. S7–S9). The degrafting rate constants of both the deuterated and hydrogenated components were then calculated as described in the previous section and are reported in Fig. 5 as a function of  $\Sigma_{TOT}$ . The presence of two regimes of degrafting is confirmed, even for disperse brushes. In fact, beyond a certain critical value of  $\Sigma_{TOT}$  ( $\Sigma_{TOT,c}$ ), the dependence of  $k$  on  $\Sigma_{TOT}$  is definitely more marked than in the case in which  $\Sigma_{TOT}$  is lower than  $\Sigma_{TOT,c}$ . Interestingly, for each brush composition,  $\Sigma_{TOT,c}$  of the two components has essentially the same value. Furthermore, the value  $\Sigma_{TOT,c}$  decreases as the percentage of short chains (PS<sub>d8</sub>5.2-OH) decreases from 90 to 20%. In more detail, in Brush90, the value of  $\Sigma_{TOT,c}$  is approximately the same as  $\Sigma_c$  of the single PS<sub>d8</sub>5.2-OH brush. In the same way, in Brush20,  $\Sigma_{TOT,c}$  and  $\Sigma_c$  of the single PS13-OH brush are similar. Finally, in Brush50, the value of  $\Sigma_{TOT,c}$  is between the  $\Sigma_c$  of the single PS<sub>d8</sub>5.2-OH brush and the one of the single PS13-OH brush.

In general, the overall curves representing  $k$  vs.  $\Sigma_{TOT}$  of both the components of the bimodal brushes are included between two limits, which consist of the curves obtained for the two single polymer brushes. In more detail, the curves of the bimodal brush are shifted toward the limit curve relative to the more abundant component of the brush. It is finally important to observe that, for  $\Sigma_{TOT} > \Sigma_{TOT,c}$ , the  $k$  of PS13-OH is systematically higher than the  $k$  of PS<sub>d8</sub>5.2-OH, indicating a faster degrafting of the longest component of the brush. The preferential detachment of the longest components of disperse brushes is in good accordance with the literature.<sup>64</sup>

The main conclusion emerging from the data presented in Fig. 5 regards the presence of mutual interactions between short and long chains. For example, a single  $\Sigma_{TOT,c}$  for PS<sub>d8</sub>5.2-OH and PS13-OH in each brush is observed. This means that the value of  $\Sigma_{TOT}$  at which the overall brush experiences tension is determined by mixed contacts between short and long polymers. Furthermore, for Brush20, the  $k$  of PS<sub>d8</sub>5.2-OH increases up to the value typical of PS13-OH. On the other side, in Brush90, the  $k$  of PS13-OH decreases to the value typical of PS<sub>d8</sub>5.2-OH. Therefore, in both cases, the minor component of the brush is forced by the interactions with the major components to assume a tension state typical of the latter, thus indicating interdependent dynamics.

**Table 1** Target molar percentage of PS<sub>d8</sub>5.2-OH, thickness ( $H_0$ ), grafting density of the PS<sub>d8</sub>5.2-OH component ( $\Sigma_{D,0}$ ), grafting density of the PS13-OH component ( $\Sigma_{H,0}$ ), total grafting density ( $\Sigma_{TOT,0}$ ) and the measured molar percentage of PS<sub>d8</sub>5.2-OH of the grafted bimodal brushes

Sample	% PS <sub>d8</sub> 5.2-OH target	$H_0$ (nm)	$\Sigma_{D,0}$ (chains per nm <sup>2</sup> )	$\Sigma_{H,0}$ (chains per nm <sup>2</sup> )	$\Sigma_{TOT,0}$ (chains nm <sup>-2</sup> )	% PS <sub>d8</sub> 5.2-OH measured
Brush90/10	90	4.7	0.44	0.05	0.49	88
Brush50/50	50	6.1	0.24	0.20	0.44	54
Brush20/80	20	7.4	0.07	0.33	0.40	19



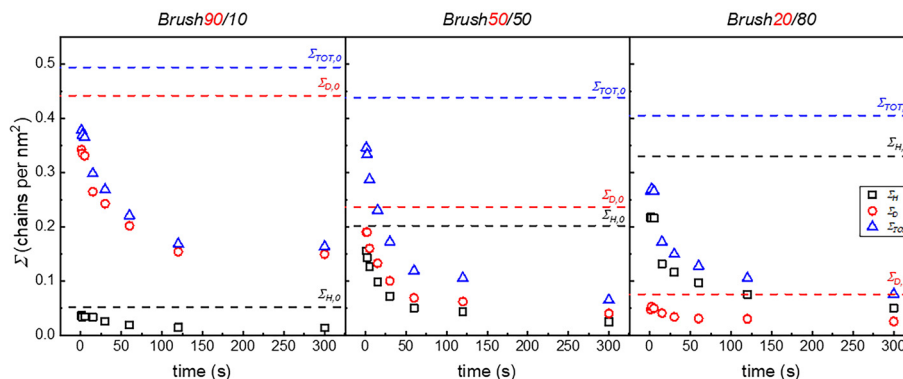


**Fig. 4**  $\Sigma_D$ ,  $\Sigma_H$  and  $\Sigma_{TOT}$  as a function of the degrafting time for the brushes Brush90, Brush50 and Brush20. The values of  $\Sigma_{D,0}$ ,  $\Sigma_{H,0}$  and  $\Sigma_{TOT,0}$  relative to the brushes before degrafting, are also included as dashed lines.



**Fig. 5**  $k$  vs.  $\Sigma_{TOT}$  for the degrafting reaction of PS<sub>d85.2</sub>-OH (dashed red line) and PS13-OH (dashed black line) in Brush90, Brush50 and Brush20. The curves representing  $k$  vs.  $\Sigma$  for the degrafting reaction in the single polymer brushes (see Fig. 3(b)) are also included as references, with a full red line for PS<sub>d85.2</sub>-OH and a full black line for PS13-OH.

The above pieces of evidence further confirm that the degree of tension, and consequently  $k$ , of a polymer in a brush is not only determined by the molecular weight and the grafting density but also by the brush composition and dispersity, with the overall degrafting kinetics complying with one of the major components.

## Conclusions

The degrafting reaction of polymer brushes constituted by two polystyrene samples with different molecular weights and related blends with different compositions was evaluated in a THF/water mixture. In all cases, a clear dependence of the degrafting rate constant on the grafting density of the brush was observed. In particular, the degrafting rate constant decreases linearly as the grafting density of the brush decreases with a sharp slope change corresponding to a critical grafting density value. For grafting densities lower than the critical value, the degrafting rate constant decreases slowly as the grafting density decreases. In contrast, when the grafting density is higher than the critical value, the degrafting rate

constant decreases steeply. This behavior suggests the presence of two distinct regimes corresponding to tensioned and relaxed polymer chains in the brush. Furthermore, the critical grafting density value depends on the molecular weight of the polymer forming the brush. In addition, and in contrast to theoretical prediction, in the range of grafting densities investigated, the degrafting of long polymer chains is faster than the degrafting of short ones. When brushes are prepared from blends of the two polystyrene samples with low and high molecular weights, the degrafting reaction of both components results in a similar product to the one of the major species in the blend.

This evidence suggests a mutual influence between the polymer chains in the brush, thus underscoring the cooperative nature of the degrafting mechanism. The overall picture provided by this work increases the understanding of the polymer brush stability, thus making it possible to produce adaptable surfaces able to change their structure and composition in a controlled way when applied in specific environments. Furthermore, these data indicate the potential to create brush layers with customized responsiveness to external stimuli associated with specific environments, rendering them



suitable for the fabrication of sensors to monitor detrimental environmental modifications and expanding the scope of applications for polymer brush layers.

## Experimental section

### Materials

The deuterated (PS<sub>d8</sub>5.2-OH) and hydrogenated (PS13-OH) polystyrenes were synthesized by ARGET-ATRP using 2-hydroxyethyl-2-bromoisobutyrate (HEBIB) as the initiator to introduce a hydroxyl functionality in the polymer end-group. All the details of the synthesis and characterization were already published.<sup>45</sup> All the reagents were purchased from Merck and used as received. P-type Czochralski-grown Si(100) wafers (a nominal resistivity of 1–5 Ω cm) were purchased from Siltronix.

### PS43.2-OH synthesis and characterization

The sample was synthesized by a two-step procedure. Firstly, a hydroxy-terminated polystyrene with  $M_n = 25.4 \text{ kg mol}^{-1}$  ( $D = 1.12$ ) was synthesized by ARGET-ATRP using 2-hydroxyethyl-2-bromoisobutyrate (HEBIB) as the initiator. More details of the synthesis and polymer characterization are reported in the literature.<sup>42</sup> The molecular weight of this polymer was then increased by using it as a macroinitiator for a second ARGET-ATRP step.<sup>41</sup> In detail, 1.5 g of the macroinitiator (59 μmol) was dissolved in a mixture consisting of 2 mL of styrene (monomer, 18 mmol, 300 equivalents), 526.3 μg of CuBr<sub>2</sub> (catalyst, 2.36 μmol, 0.04 equivalents), 0.6 μL of tris[2-(dimethylamino)ethyl]amine (ligand, 2.36 μmol, 0.04 equivalents) and 2 mL of anisole (solvent). The mixture was transferred to a Schlenk flask and degassed by two freeze-thaw cycles. After that, a solution consisting of 9.5 mg of tin(II) 2-ethylhexanoate (reducing agent, 23.6 μmol, 0.4 equivalents), 6 μL of tris[2-(dimethylamino)ethyl]amine (ligand, 23.6 μmol, 0.4 equivalents) and 1 mL of anisole was added to the mixture and a further freeze-thaw cycle was performed. The reaction was carried out at 90 °C in a thermostatic oil bath for 17 h. The polymer was then purified by two successive precipitations carried out with a THF polymer solution in cold methanol. The  $M_n$  and  $D$  values of PS43.2-OH were determined by Size Exclusion Chromatography (SEC). The analysis was performed with a 590 Waters chromatograph equipped with Waters HSPgel HR3 and HR4 columns and a refractive index detector. The eluent was THF, while the flow rate was 0.3 mL min<sup>-1</sup>. The instrument was calibrated with polystyrene standards with molecular weights ranging from 1 to 100 kg mol<sup>-1</sup>. The PS43.2-OH chromatograph is reported in Fig. S10.

### Grafting procedure

All the polymer brushes were obtained with the same procedure.<sup>68,69</sup> Silicon wafers covered with an ~2 nm thick layer of native oxide were cut into slices of 1 cm × 1 cm, treated with piranha solution (H<sub>2</sub>SO<sub>4</sub>/H<sub>2</sub>O<sub>2</sub> 3/1 volume ratio) for 40 min at 80 °C, rinsed with deionized water and dried under

a nitrogen flow. The wafers were then washed with 2-propanol for 15 min in a sonication bath and dried under a nitrogen flow. An ~30 nm thick layer of the polymer was deposited onto the wafer by spin-coating (3000 rpm, 30 s). The polymer solutions used for the spin-coating process are reported in Table 2.

The grafting to reaction of the deposited polymers was performed on a SAWATEC HP-150 hot plate placed in a MBRAUN LABstar glovebox (inert atmosphere, H<sub>2</sub>O, O<sub>2</sub> < 1 ppm). The reaction was carried out at 250 °C for 900 s. The unreacted chains were removed by toluene washes carried out in a sonication bath for 5 min. The wafers were finally dried under a nitrogen flow.

### Degrafting procedure

The sample was immersed in a mixture containing 75% THF and 25% buffer solution pH = 10 (boric acid/potassium chloride/sodium hydroxide). The reaction was carried out at room temperature for different times. The samples were then rinsed with deionized water, dried under a nitrogen flow, rinsed with fresh THF for 5 min and dried again under a nitrogen flow.

### Brush characterization

The brush thickness was measured using a FS-1 multiwavelength ellipsometer (Film Sense). The error of the measurement was seen to be less than 0.1 nm.

The composition of the bimodal brush was evaluated by TGA-GC-MS analysis. The TGA instrument was a Mettler Toledo TGA/DSC 3+ model, while the GC-MS apparatus was a Finnigan GC Trace 1300 MS ISQ LT instrument equipped with a Phenomenex DB5-5MS capillary column of 30 m of length, 0.25 mm of inner diameter and 0.25 μm of thickness. The sample was annealed in the TGA oven from 25 to 1000 °C with a heating ramp of 20 °C min<sup>-1</sup> under a helium flow (50 mL min<sup>-1</sup>). The degradation products were collected and introduced in the GC-MS instrument. The signals revealed in the MS were acquired in EI+ mode in the Selected Ion Monitoring (SIM) mode, with specific focus on the species with  $m/z$  of 104 and 112, relative to styrene and deuterated styrene monomers respectively. More details on this hyphenated technique, including the temperatures of the transfer lines and the various segments, are published elsewhere.<sup>71,73</sup>

The areas of the signals relative to the species with  $m/z$  of 104 and 112, indicated as  $A_{\text{STY}}$  and  $A_{\text{STYd8}}$ , were demonstrated to be proportional to the molar amount of styrene and deuterated styrene in the analyzed brush.<sup>45</sup> The mass fraction of

**Table 2** Composition of the solutions used in the spin-coating process. The amounts of PS<sub>d8</sub>5.2-OH, PS13-OH and toluene (solvent) for each typology of brush are reported

Brush	PS <sub>d8</sub> 5.2-OH (mg)	PS13-OH (mg)	Toluene (mL)
Single PS <sub>d8</sub> 5.2-OH	9.0		1
Single PS13-OH		9.0	1
Brush90	6.2	2.8	1
Brush50	1.8	7.2	1
Brush20	0.5	8.5	1



styrene ( $F_{\text{PS13-OH}}$ ) in the brush is then calculated using eqn (5).<sup>45</sup>

$$F_{\text{PS13-OH}} = \frac{A_{\text{STY104}}}{A_{\text{STY104}} + A_{\text{STYd8112}}} \quad (5)$$

Finally, the grafting density of the deuterated  $\text{PS}_{\text{d8}}5.2\text{-OH}$  polymer ( $\Sigma_{\text{D}}$ ) and the hydrogenated PS13-OH polymer ( $\Sigma_{\text{H}}$ ) and the total grafting density ( $\Sigma_{\text{TOT}}$ ) were calculated using the following equations:<sup>45</sup>

$$\Sigma_{\text{D}} = \frac{(1 - F_{\text{PS13-OH}})HdN_{\text{A}}}{5200} \quad (6)$$

$$\Sigma_{\text{H}} = \frac{F_{\text{PS13-OH}}HdN_{\text{A}}}{13\,000} \quad (7)$$

$$\Sigma_{\text{TOT}} = \Sigma_{\text{D}} + \Sigma_{\text{H}} \quad (8)$$

## Conflicts of interest

There are no conflicts to declare.

## Data availability

The data that support this work are available in the main text and in the supplementary information (SI). Supplementary information is available. See DOI: <https://doi.org/10.1039/d5py01210d>.

## Acknowledgements

We acknowledge Professor Giuseppe Milano for the fruitful exchange of opinions that took place during the research work and the analysis of the data.

## References

- 1 A. S. Goldmann, N. R. B. Boase, L. Michalek, J. P. Blinco, A. Welle and C. Barner-Kowollik, *Adv. Mater.*, 2019, **31**, 1–21.
- 2 S. V. Orski, K. H. Fries, S. K. Sontag and J. Locklin, *J. Mater. Chem.*, 2011, **21**, 14135–14149.
- 3 W. L. Chen, R. Cordero, H. Tran and C. K. Ober, *Macromolecules*, 2017, **50**, 4089–4113.
- 4 W. J. Brittain and S. Minko, *J. Polym. Sci., Part A: Polym. Chem.*, 2007, **45**, 3505–3512.
- 5 H. Liu, Y. Li, K. Sun, J. Fan, P. Zhang, J. Meng, S. Wang and L. Jiang, *J. Am. Chem. Soc.*, 2013, **135**, 7603–7609.
- 6 N. Fortin and H. Klok, *ACS Appl. Mater. Interfaces*, 2015, **7**, 4631–4640.
- 7 L. A. Smook, G. C. Ritsema van Eck and S. de Beer, *ACS Appl. Polym. Mater.*, 2021, **3**, 2336–2340.
- 8 E. Han, K. O. Stuen, M. Leolukman, C. C. Liu, P. F. Nealey and P. Gopalan, *Macromolecules*, 2009, **42**, 4896–4901.
- 9 F. Ferrarese Lupi, T. J. Giammaria, F. G. Volpe, F. Lotto, G. Seguin, B. Pivac, M. Laus and M. Perego, *ACS Appl. Mater. Interfaces*, 2014, **6**, 21389–21396.
- 10 S. Wang, Z. Wang, J. Li, L. Li and W. Hu, *Mater. Chem. Front.*, 2020, **4**, 692–714.
- 11 S. Wang, Z. Wang, Y. Huang, Y. Hu, L. Yuan, S. Guo, L. Zheng, M. Chen, C. Yang, Y. Zheng, J. Qi, L. Yu, H. Li, W. Wang, D. Ji, X. Chen, J. Li, L. Li and W. Hu, *ACS Appl. Mater. Interfaces*, 2021, **13**, 17852–17860.
- 12 R. Chiarcos, M. Laus and M. Perego, *Eur. Polym. J.*, 2024, **208**, 112849.
- 13 J. J. Keating IV, J. Imbrogno and G. Belfort, *ACS Appl. Mater. Interfaces*, 2016, **8**, 28383–28399.
- 14 E. Nur Durmaz, S. Sahin, E. Virga, S. de Beer, L. C. P. M. de Smet and W. M. de Vos, *ACS Appl. Polym. Mater.*, 2021, **3**, 4347–4374.
- 15 K. B. Buhl, A. H. Agergaard, M. Lillethorup, J. P. Nikolajsen, S. U. Pedersen and K. Daasbjerg, *Polymers*, 2020, **12**, 1475.
- 16 Y. Yu, M. B. Pérez, C. Cao and S. de Beer, *Eur. Polym. J.*, 2021, **147**, 110298.
- 17 J. M. Giussi, M. Lorena Cortez, W. A. Marmisolle and O. Azzaroni, *Chem. Soc. Rev.*, 2019, **48**, 814–849.
- 18 T. Kreer, *Soft Matter*, 2016, **12**, 3479–3501.
- 19 J. Klein, E. Kumacheva, D. Mahalu, D. Perahla and L. J. Fetters, *Nature*, 1994, **370**, 634–636.
- 20 S. De Beer, E. Kutnyanszky, P. M. Schon, G. J. Vancso and M. H. Muser, *Nat. Commun.*, 2014, **5**, 3781.
- 21 W. Yan, S. N. Ramakrishna, N. D. Spencer and E. M. Benetti, *Langmuir*, 2019, **35**, 11255–11264.
- 22 K. Ishihara, *Langmuir*, 2019, **35**, 1778–1787.
- 23 C. Yoshikawa, S. Hattori, C.-F. Huang, H. Kobayashi and M. Tanaka, *J. Mater. Chem. B*, 2021, **9**, 5794–5804.
- 24 M. Welch, A. Rastogi and C. Ober, *Soft Matter*, 2011, **7**, 297–302.
- 25 L. Li, S. Chen, J. Zheng, B. D. Ratner and S. Jiang, *J. Phys. Chem. B*, 2005, **109**, 2934–2941.
- 26 M. Kim, S. K. Schmitt, J. W. Choi, J. D. Krutty and P. Gopalan, *Polymers*, 2015, **7**, 1346–1378.
- 27 Z. Ding, C. Chen, Y. Yu and S. de Beer, *J. Mater. Chem. B*, 2022, **10**, 2430–2443.
- 28 J. O. Zoppe, N. C. Ataman, P. Mocny, J. Wang, J. Moraes and H. A. Klok, *Chem. Rev.*, 2017, **117**, 1105–1318.
- 29 S. Edmondson, V. L. Osborne and W. T. S. Huck, *Chem. Soc. Rev.*, 2004, **33**, 14–22.
- 30 J. Pyun, T. Kowalewski and K. Matyjaszewski, *Macromol. Rapid Commun.*, 2003, **24**, 1043–1059.
- 31 B. Zhao and W. J. Brittain, *Prog. Polym. Sci.*, 2000, **25**, 677–710.
- 32 R. Barbey, L. Lavanant, D. Paripovic, N. Schuwer, C. Sugnaux, S. Tugulu and H. Klok, *Chem. Rev.*, 2009, **109**, 5437–5527.
- 33 C. M. Hui, J. Pietrasik, M. Schmitt, C. Mahoney, J. Choi, M. R. Bockstaller and K. Matyjaszewski, *Chem. Mater.*, 2014, **26**, 745–762.
- 34 H. Klok and J. Genzer, *ACS Macro Lett.*, 2015, **4**, 636–639.



- 35 B. Zdyrko and I. Luzinov, *Macromol. Rapid Commun.*, 2011, **32**, 859–869.
- 36 R. Chiarcos, M. Perego and M. Laus, *Macromol. Chem. Phys.*, 2023, **224**, 2200400.
- 37 L. J. Norton, V. Smigolova, M. U. Pralle, A. Hubenko, K. H. Dai, E. J. Kramer, S. Hahn, C. Berglund and B. Dekoven, *Macromolecules*, 1995, **28**, 1999–2008.
- 38 P. Mansky, Y. Liu, E. Huang, T. P. Russell and C. Hawker, *Science*, 1997, **275**, 1458–1460.
- 39 K. S. Iyer, B. Zdyrko, H. Malz, J. Pionteck and I. Luzinov, *Macromolecules*, 2003, **36**, 6519–6526.
- 40 K. Viswanathan, T. E. Long and T. C. Ward, *J. Polym. Sci., Part A: Polym. Chem.*, 2005, **43**, 3655–3666.
- 41 K. Sparnacci, D. Antonioli, V. Gianotti, M. Laus, F. F. Lupi, T. J. Giammaria, G. Seguini and M. Perego, *ACS Appl. Mater. Interfaces*, 2015, **7**, 10944–10951.
- 42 M. Perego, G. Seguini, E. Arduca, A. Nomellini, K. Sparnacci, D. Antonioli, V. Gianotti and M. Laus, *ACS Nano*, 2018, **12**, 178–186.
- 43 V. M. Ospina, R. Chiarcos, D. Antonioli, V. Gianotti, M. Laus, S. Kuschlan, C. Wiemer and M. Perego, *ACS Appl. Electron. Mater.*, 2022, **4**, 6029–6037.
- 44 M. Laus, R. Chiarcos, V. Gianotti, D. Antonioli, K. Sparnacci, G. Munaò, G. Milano, A. De Nicola and M. Perego, *Macromolecules*, 2021, **54**, 499–508.
- 45 R. Chiarcos, D. Antonioli, A. Baldanza, C. Brondi, G. Munaò, G. Milano, M. Laus and M. Perego, *Macromolecules*, 2025, **58**, 1935–1949.
- 46 C. Ivaldi, V. O. M. Guarin, D. Antonioli, G. Zuccheri, K. Sparnacci, V. Gianotti, M. Perego, R. Chiarcos and M. Laus, *Macromol. Rapid Commun.*, 2024, **45**, 2400288.
- 47 Y. Zhang, J. He, Y. Zhu, H. Chen and H. Ma, *Chem. Commun.*, 2011, **47**, 1190–1192.
- 48 Y. Zhu, B. Lv, P. Zhang and H. Ma, *Chem. Commun.*, 2011, **47**, 9855–9857.
- 49 H. A. Klok and J. Genzer, *ACS Macro Lett.*, 2015, **4**, 636–639.
- 50 S. Tugulu and H. Klok, *Biomacromolecules*, 2008, **9**, 906–912.
- 51 N. C. Ataman and H. Klok, *Macromolecules*, 2016, **49**, 9035–9047.
- 52 Y. Ko and J. Genzer, *Macromolecules*, 2019, **52**, 6192–6200.
- 53 E. D. Bain, K. Dawes, A. O. Evren, X. Hu, C. B. Gorman, J. Srogl and J. Genzer, *Macromolecules*, 2012, **45**, 3802–3815.
- 54 D. Paripovic and H. Klok, *Macromol. Chem. Phys.*, 2011, **212**, 950–958.
- 55 R. Quintana, M. Gosa, D. Jan, E. Kutnyanszky and G. J. Vancso, *Langmuir*, 2013, **29**, 10859–10867.
- 56 M. B. Perez, M. Cirelli and S. De Beer, *ACS Appl. Polym. Mater.*, 2020, **2**, 3039–3043.
- 57 F. Wang, W. Liu, R. Lu, J. Huang, B. Zuo and X. Wang, *ACS Macro Lett*, 2022, **11**, 1041–1048.
- 58 P. G. de Gennes, *Macromolecules*, 1980, **13**, 1069–1075.
- 59 Z. Frakas, I. Derenyi and T. Vicsek, *J. Phys.: Condens. Matter*, 2003, **15**, 1767–1777.
- 60 S. Panyukov, E. B. Zhulina, S. S. Sheiko, G. C. Randall, J. Brock and M. Rubinstein, *J. Phys. Chem. B*, 2009, **113**, 3750–3768.
- 61 S. S. Sheiko, S. Panyukov and M. Rubinstein, *Macromolecules*, 2011, **44**, 4520–4529.
- 62 L. Léger, E. Raphaël and H. Hervet, *Adv. Polym. Sci.*, 1999, **138**, 186–225.
- 63 J. Wang and H. Klok, *Angew. Chem., Int. Ed.*, 2019, **58**, 9989–9993.
- 64 K. A. Melzak, K. Yu, D. Bo, J. N. Kizhakkedathu and J. L. Toca-herrera, *Langmuir*, 2015, **31**, 6463–6470.
- 65 S. Sant, K. Kaur and H. Klok, *Langmuir*, 2024, **40**, 21656–21662.
- 66 W. Jakubowski, K. Min and K. Matyjaszewski, *Macromolecules*, 2006, **39**, 39–45.
- 67 L. Michalek, L. Barner and C. Barner-Kowollik, *Adv. Mater.*, 2018, **30**, 1–18.
- 68 D. Antonioli, R. Chiarcos, V. Gianotti, M. Terragno, M. Laus, G. Munaò, G. Milano, A. De Nicola and M. Perego, *Polym. Chem.*, 2021, **12**, 6538–6547.
- 69 R. Chiarcos, D. Antonioli, V. Gianotti, M. Laus, G. Munaò, G. Milano, A. De Nicola and M. Perego, *Polym. Chem.*, 2022, **13**, 3904–3914.
- 70 R. Chiarcos, D. Antonioli, V. Ospina, M. Laus, M. Perego and V. Gianotti, *Analyst*, 2021, **146**, 6145–6155.
- 71 D. Antonioli, K. Sparnacci, M. Laus, F. Ferrarese Lupi, T. J. Giammaria, G. Seguini, M. Ceresoli, M. Perego and V. Gianotti, *Anal. Bioanal. Chem.*, 2016, **408**, 3155–3163.
- 72 R. Chiarcos, D. Antonioli, E. Podda, G. Muna, G. Milano, M. Perego and M. Laus, *Polymer*, 2025, **335**, 128804.
- 73 V. Gianotti, D. Antonioli, K. Sparnacci, M. Laus, J. T. Giammaria, M. Ceresoli, F. Ferrarese Lupi, G. Seguini and M. Perego, *J. Chromatogr. A*, 2014, **1368**, 204–210.

